北海道大学工学部研究報告
第164号（平成5年）

Bulletin of the Faculty of Engineering
Hokkaido University No. 164 (1993)

Fractography of Translaminar Fractures of Carbon Fiber Reinforced Plastics

Toru NOGUCHI*, Ken NARUSE**,
and Eiki TSUSHIMA***

(Received December 21, 1992)

Abstract

The fracture morphology of continuous fiber reinforced composites is very complicated and it is difficult to estimate the fracture process by fractography. In this report, translaminar type fracture of continuous carbon fiber composite was investigated, and it was attempted to determine indicators of fracture path, fracture origines, and loading conditions by SEM fractography. Three types of model specimens and two types of bulk specimens were fractured by static and impact bending. Fractured surface was examined by SEM, and microscopic fracture appearance was related to macroscopic fracture features.

In high magnification observations, the local crack direction can be determined by mapping of the radial mark direction on broken fiber ends, tension-compression boundary lines in buckled fibers and other microscopic morphologic features. For failure analysis, however, low magnification observation is more effective; the overall fracture direction and fracture initiation region can be estimated from macroscopic ridge marks, micro-buckling bands, and intralaminar shear cracks, and these estimates are confirmed by higher magnification observations.

1. Introduction

Fractography is an important technique for structural materials because it is often applied to investigate causes of material failures and as it provides feedback to the structural design and fabrication stages. Fractography is well established in metals[1], but in composite materials it is not applied successfully due to the complexity of the fracture morphologies. Particularly in continuous fiber reinforced composite, the fracture surface is extremely rough because these are many types of fractures as translaminar, intralaminar, interlaminar, and combinations of these[2-4], and this makes it very difficult to trace the main crack path and determine the origin of fractures. It has been stressed

* Dept. of Mechanical Engineering II, Faculty of Engineering, Hokkaido University, Sapporo 060 Japan.
** Graduate student, now in Mei-Tech Co., Isehara, Kanagawa Prefecture.
*** Tohnen Co., Research Center, Ooi, Saitama Prefecture.

that experience and patience are required in examining particularly this type of fracture[4].

The research here attempted to establish clues for determining the load type, the way of propagation and the origin of the fracture in translaminar type fractures, with fundamental fractography performed on carbon fiber reinforced plastic (CFRP) specimens. The microscopic features of broken fibers and the surrounding matrix was related to the low magnification fracture appearance and the macroscopic fracture conditions.

2. Experiment

Continuous fiber composites desplay three types of fracture[4]: intralaminar, where the separation occurs along the fiber direction (Fig. 1-(2)): interlaminar, where the separation is between fiber plys (Fig. 1-(3)), and translaminar, where the fracture occurs perpendicular to and cuts the fibers (Fig. 1-(1)). This last type of fracture surface shows extremely complicated features.

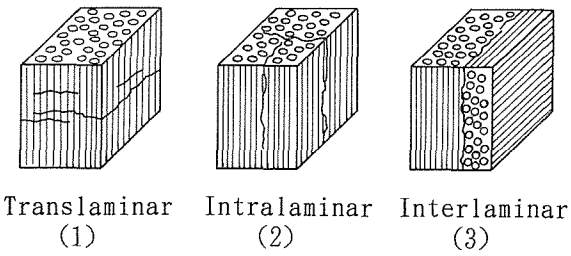

Fig. 1 Fracture types in continuous fiber composites.

The experiments used high strength PAN type carbon fiber, Torayca T300, with tree types of model specimens and two bulk specimens prepared with continuous carbon fibers and epoxy resin. A bending load was applied perpendicular to the fiber direction to create translaminar type tractures.

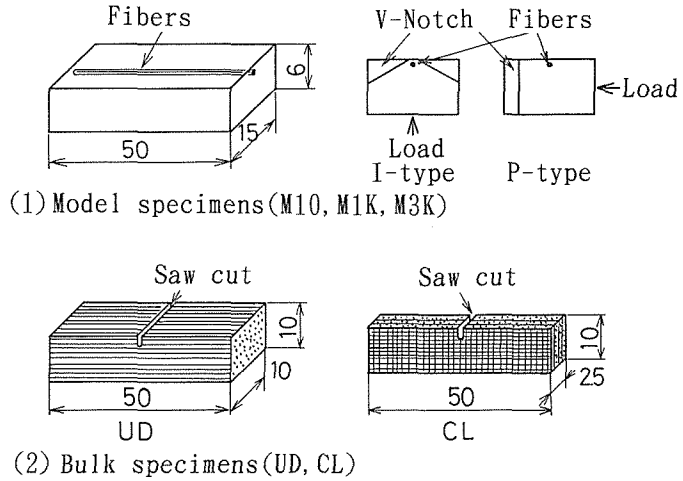

Fig. 2 Specimens, (1) model specimens (M 10, M 1 K, M 3 K) and (2) bulk specimens (UD, CL).

The model speciments are 15×16×50 (mm) epoxy resin beams as shown in Fig. 2, containing 10 fibers (M10), about 1000 fibers (M1K), or 3000 fiber impregnated strands (M3K), buried just below the surface at the center of the 15mm long side. In M10, fibers were carefully removed from a 3000 fiber strand, and to adjust the tension of the fibers during the arraying for specimen casting, 1g weights (1 yen coins) were used at the fiber ends.

Specimens were fractured under two loading conditions; with fibers in the tensile surface (fracture initiation site, I-type), and with fibers in the side surface (fracture propagation site, p-type). To induce fracture initiation, slant notches were machined in both sides of the buried fibers in I-type specimens, and a 2mm deep V notch was made on the tensile side of the p-type specimens.

The bulk specimens were: UD, a 10mm thick unidirectionally reinforced specimen, and CL, a 2.5mm thick cloth reinforced specimen, both with about a 60% fiber volume fraction. They were machined to 10mm high and 50mm long bending specimens as shown in Fig. 2-(2), with a 2mm deep saw cut made on the tension side. Loading was static or impact three point bending with a 40mm suport distance. Impact bending was by a 150 N-m Charpy tester with 5m/sec impact velocity. Fractured surfaces were evaporated with Au for SEM observations.

3. Results of observations

3.1 Model specimens with 10 fibers (M10)

In M10 specimens, carbon fibers were dispersed in the matrix separated by 1-3 fiber diameters. The fracture direction was easily traced both by radial marks on the broken fiber ends and feather like marks in the matrix resin. An example where the fracture origin can be determined in an I-type specimen is in Fig. 3-(1). Here the fracture surface of matrix and fiber is flush, indicating that the fracture originated from a point between the two fibers. The radial marks on the right fiber shows a different fracture direction, indicating that its fracture origin is different. Fig. 3-(2) shows another fracture origin in

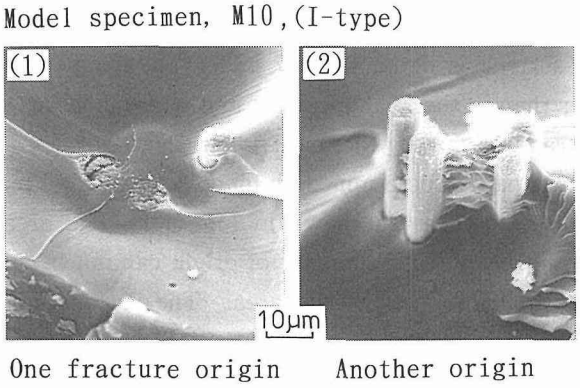

Fig. 3 Fracture origin in model specimen M 10, Static loading.

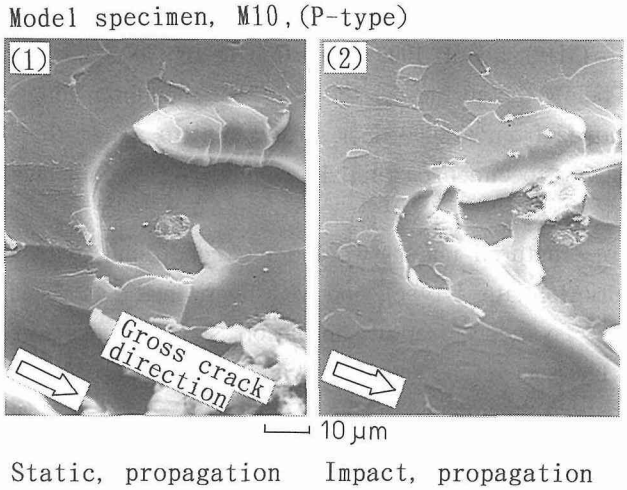

Fig. 4 Fracture surface of model specimen, M 10, P-type, (1) static loading and (2) impact loading.

the same surface, with some fibers protruding. It suggests that the fracture originated in multiple sites even in this very simple 10 fiber composite model.

In p-type M10 specimens, parabolic marks form in the matrix around the fibers, indicating interaction between the main crack and cracks originating from fiber breakage[5]. The axis of the parabolic marks that indicate the direction of local fracture propagation coincides with the gross crack orientation in most of the fibers, as shown in Fig. 4-(1). However in some fibers, they did not coincide.

Impact fractures showed similar, but generally, flatter fracture surfaces with shorter pulled out fibers. In the region of propagation, the matrix parabolic marks were narrower than in static fracture, as shown in Fig. 4-(2), indicating higher main crack velocities.

3.2. Model specimens with 1000 fiber strand (M1K)

An example of a fracture surface of the M1K specimen, I-type, is shown in Fig. 5 (1)-(3). The low magnification image clearly shows that the fracture originated from the fiber region, but the surface is dominated by pulled out fibers of various lengths. The matrix part is smaller than in the M10 specimen and with numerous steps, making it very difficult to trace the fracture path by the matrix markings.

The overall fracture path is determined by mapping the radial marks on the fractured ends of a group of broken fibers as shown in Fig. 5(3). The area where the fracture initiated can be determined, but a single point of origin can not be specified because many cracks initiated from multiple fibers in the area. The surface was generally flatter in impact fracture than in static fractures.

In P-type (fibers in propagation area) specimens, the direction of propagation determined by the marks on the fiber end coincides with the macroscopic fracture directions,

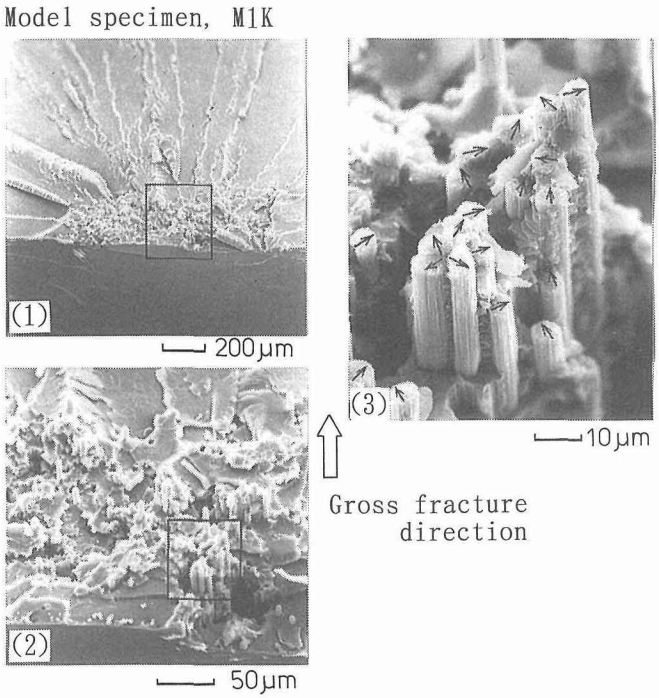

Fig. 5 Fracture surface of model specimen M1K, static loading. Arrows indicate gross crack direction.

and there were no significant differences between impact and static fractures.

3.3. Model specimens with 3K impregnated strand (M3K)

In static loading, both the I and P type M3K specimens showed delamination between the strand and matrix, translaminar fractures did not occur. The specimen fractured in the translaminar direction with impact loading, and the area where the fracture originated was determined like with the M1K specimens. Fig. 6 shows radial mark directions mapped on the fracture end of fibers in an I-type M3K specimen.

In P-type specimens, the strand buried at the middle of the specimen width was subjected to bending rather than tension. It showed characteristic features of bending fracture with tensile and compressive fracture regions as shown in Fig. 7-(1).

In low magnification, compressive frac-

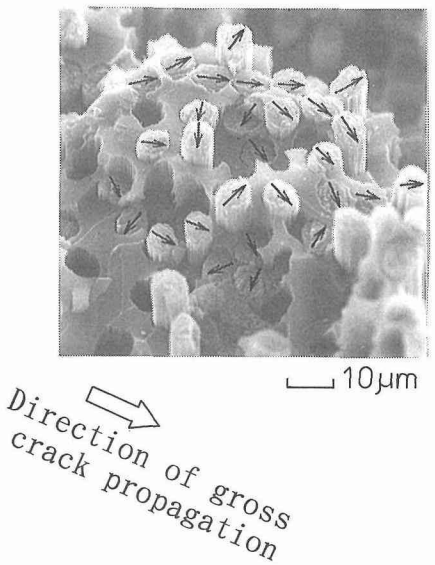

Fig. 6 Mapping of ridge mark directions in fiber ends, model specimen M1K, I-type, impact loading.

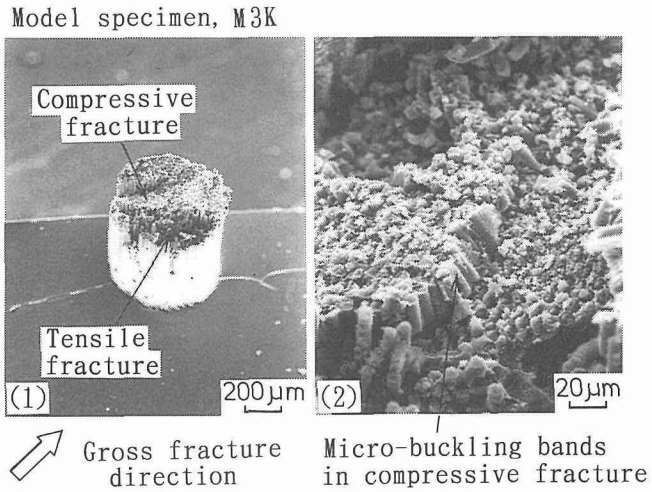

Fig. 7 Fracture surface of model specimen M3K, P-type, impact loading, (1) bending fracture of 3K strand, (2) micro-buckling bands in the compressive fracture region.

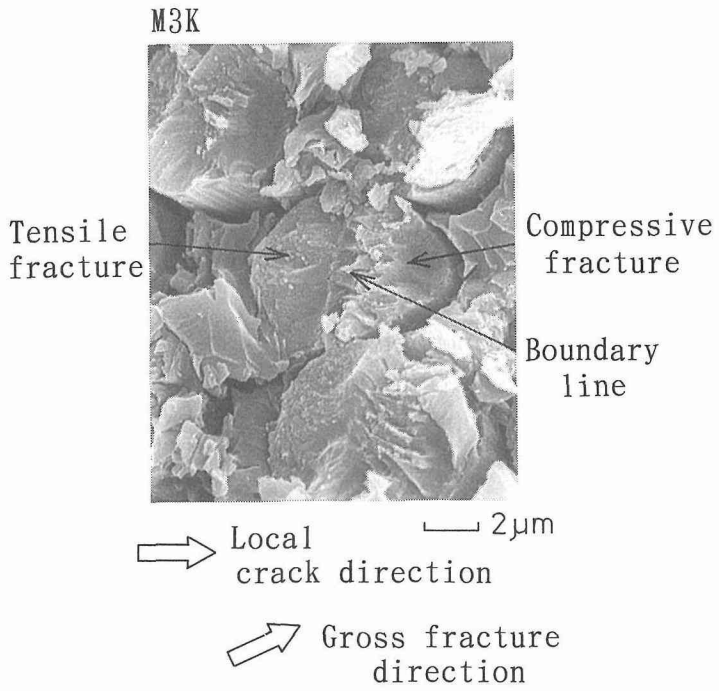

Fig. 8 Fractured fiber ends in the compressive fracture region.

tures can be identified by a rather flat surface[6], and at higher magnification by micro-buckling bands like in Fig. 7-(2). Each fractured fiber ends in a buckled area consisting of a tensile fracture region and a compression damaged region separated by a clear boundary line as seen in Fig. 8. The direction of the separating line is transverse to the direction of the fiber ending and generally coincides with the gross fracture direction, but

is not always exactly equal. Occasionally, post fracture damage makes it difficult to determine the fracture direction in the compressive fracture region.

3.4. Unidirectionally reinforced bulk specimen (UD)

In UD specimens, overall crack initiation and propagation could be detected by low magnification SEM observations as in Fig. 9-(1) and (2). Fig. 9-(1) is a static fracture. Directly below the saw cut, these is a relatively flat fracture surface with ridge marks similar to the chevron pattern in brittle fracture of steels. High magnification observations showed radial marks on the fractured end of fibers, and the direction generally coincides with the gross direction of fracture propagation.

In static specimens, the tensile area was less than 1mm from the saw cut and most of the other parts showed features of compressive fracture with a flat compressive damage area, micro-buckling and intralaminar cracks. In the impact fracture in Fig. 9-(2), the tensile fracture area is larger than in the static fracture. Ridge marks on broken fibers shown by high magnification generally indicated the same direction as the overall fracture. With increasing distance from the saw cut, the surface roughness increases with numberous pulled out fibers and intralaminar shear, followed by a compressive fracture region. After the compressive fracture and clear intralaminar shear fracture zone, there is a further tensile fracture region followed by a compressive fracture region. This shows that the impact bending in Fig. 9-(2) is a combination of two bent parts bounded by intralaminar shear fracture, as shown schematically in Fig. 10-(2).

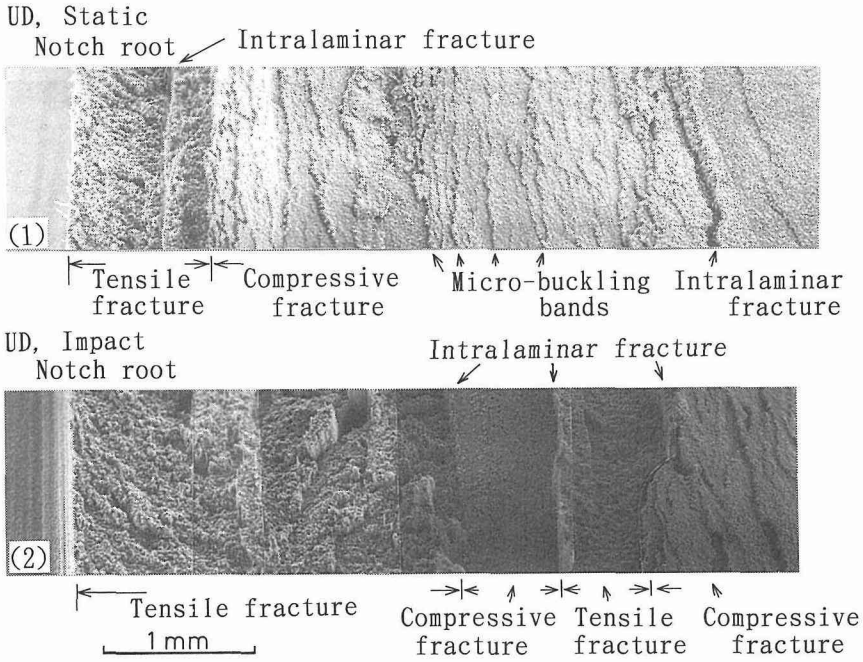

Fig. 9 Fracture surface of unidirectional specimens, (1) static loading and, (2) impact loading.

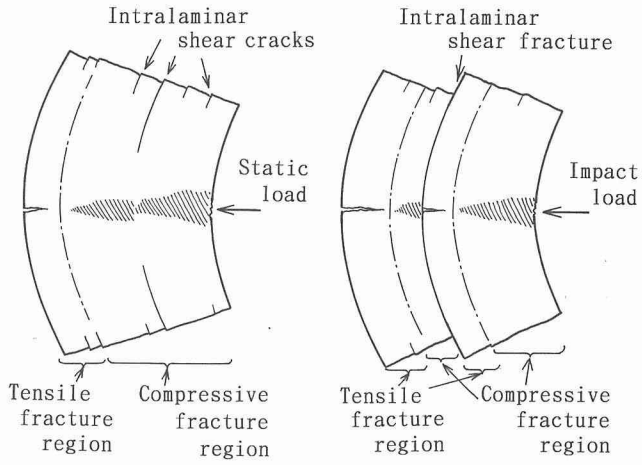

Fig. 10 Sketch of bending fractures causing the fracture surfaces in Fig. 9-(1), static, and (2), impact.

3.5. Cloth reiforced specimens (CL)

Fig. 11 shows the fracture surface of CL specimens, (1) is by static loading and (2) is by impact loading. Translaminar fracture occurs more easily than in unidirectional specimens because the fracture path is constrained by lateral fiber strands. Although half of the surface is covered by delaminated lateral strands, most axial strands show translaminar fracture. The fracture shows features similar to those observed in UD specimens, at low magnification, there are ridge marks, pulled off fibers, delamination, and a flat compressive fracture region. The fracture origin and path can be determined like in

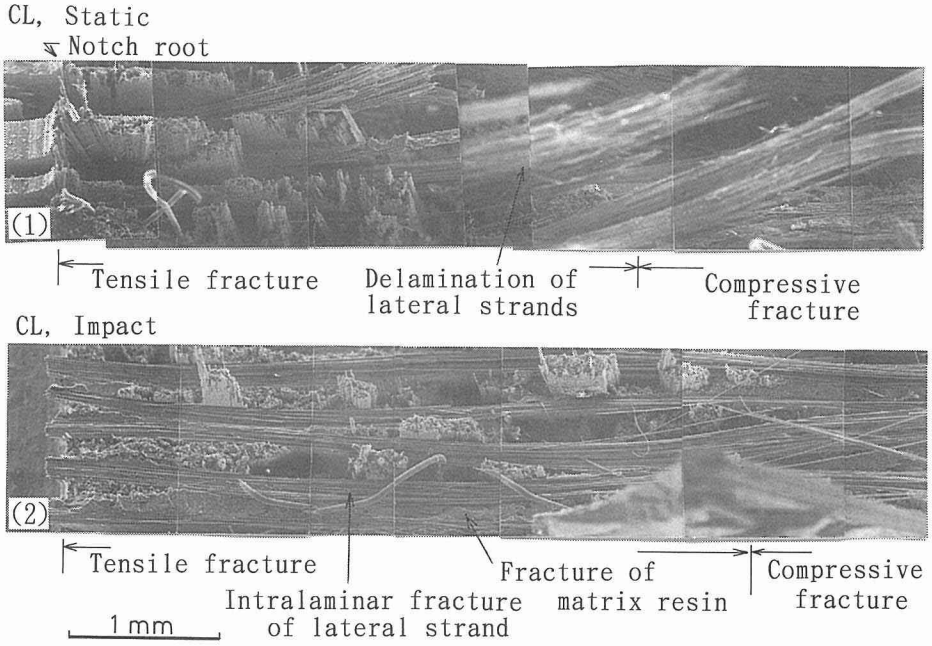

Fig. 11 Fracture surface of cloth reinforced speciments, (1) static loading and, (2) impact loading.

UD specimens. The tensile fracture region is wider in impact fracture than in static fracture.

4. Pitch type CFRP

Fig. 12 is an example of a fracture surface of pitch type CFRP. The specimen is an impregnated 3000 fiber strand fractured in a tensile test. The ridge marks on the broken

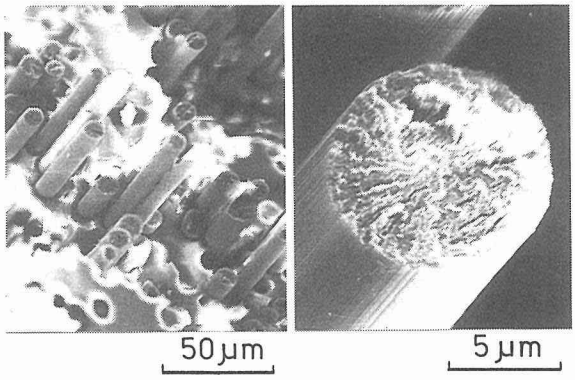

Fig. 12 Fracture surface in pitch type CFRP, 3K fiber impregnated strand, static tension.

fiber ends show radial lines. However, these lines only indicate the radial structure of fibers and do not indicate fracture directions. High magnification observations do not help in determining the gross fracture orientation. Fracture features observed at low magnification may be suitable to estimate the fracture path and fracture origins.

5. Conclusions

Model and bulk specimens of CFRP were subjected to SEM fractography on translaminar fractures. Microscopic fracture morphologies were related to the macroscopic fracture paths, origins and loading types. The fracture surface is very complicated with numerous pulled out fibers, matrix steps, and fiber-matrix delaminations in translaminar fractures, but careful examination still allows a determination of the fracture initiation region and the fracture process.

For failure investigations, low magnification SEM observation generally offers the most effective information of the overall fracture, which may be confirmed with more precise observations of and around each broken fiber by high magnification SEM. The roughness of the fracture surface, macroscopic ridge marks, protrusion length, intralaminar cracks, and direction of micro-buckling bands are clues in visual and low magnification SEM. Radial marks on broken fiber ends, feather and parabolic marks in the matrix when the fiber fraction is low, and the direction of tension-compression boundary lines, are important features in high magnification SEM observations.

More extensive use of high performance composites in important structural parts

requires that a reliable system of fractography techniques be established.

Acknowledgement

The SEM observations in this research was performed in the High Voltage Electron Microscope Laboratory of Hokkaido University, and the authors wish to express their gratitude for the assistance extended by the staff of that facility.

Referenses

1) ASM Metals Handbook 9th Ed. vol. 12 (Fractography), (1987), ASM (Metals Park, Ohio)
2) P. S. Theocaris, C. A. Stassinakis, J. of Composite Materials, 15 (1981), 133
3) W. D. Basom, D. J. Boll, et. al. J. of Materials Science, 20 (1985), 3184
4) B. W. Smith, R. A. Grove, ASM Metals Handbook 9th Ed. vol. 11 (1986), 731, ASM (Metals Park, Ohio).
5) I. Narisawa, Strength and Fracture of Polymers (1982), 209, Ohm (Tokyo)
6) M. G. Dobb, D. J. Johnson, C. R. Park, J. of Materials Science, 25 (1990), 829